Available online at www.sciencedirect.com
ScienceDirect
Earth and Planetary Science Letters 259 (2007) 134–148
EPSL
www.elsevier.com/locate/epsl

Ancient recycled crust beneath the Ontong Java Plateau: Isotopic evidence from the garnet clinopyroxenite xenoliths, Malaita, Solomon Islands

Akira Ishikawa *, Takeshi Kuritani, Akio Makishima, Eizo Nakamura

Pheasant Memorial Laboratory, Institute for Study of the Earth's Interior, Okayama University at Misasa, Tottori, 682-0193, Japan

Received 23 October 2006; received in revised form 17 April 2007; accepted 23 April 2007
Available online 27 April 2007
Editor: R.W. Carlson

Abstract

We present a Sr, Nd, Hf and Pb isotope investigation of a set of garnet clinopyroxenite xenoliths from Malaita, Solomon Islands in order to constrain crustal recycling in the Pacific mantle. Geological, thermobarometric and petrochemical evidence from previous studies strongly support an origin as a series of high-pressure (>3 GPa) melting residues of basaltic material incorporated in peridotite, which was derived from Pacific convective mantle related to the Ontong Java Plateau magmatism. The present study reveals isotopic variations in the pyroxenites that are best explained by different extents of chemical reaction with ambient peridotite in the context of a melting of composite source mantle. Isotopic compositions of bimineralic garnet clinopyroxenites affected by ambient peridotite fall within the oceanic basalt array, similar to those of Ontong Java Plateau lavas. In contrast, a quartz-garnet clinopyroxenite, whose major element compositions remain intact, has lower $^{206}Pb/^{204}Pb$–$^{143}Nd/^{144}Nd$ and higher $^{87}Sr/^{86}Sr$–$^{207}Pb/^{204}Pb$ ratios than most oceanic basalts. These isotopic signatures show some affinity with proposed recycled sources such as the so-called EM-1 or DUPAL types. Constraints from major and trace element characteristics of the quartz-garnet clinopyroxenite, the large extent of Hf–Nd isotopic decoupling and the good coincidence of Pb isotopes to the Stacey–Kramers curve, all indicate that pollution of southern Pacific mantle occurred by the subduction or delamination of Neoproterozoic granulitic lower crust (0.5–1 Ga). This crustal recycling could have taken place around the suture of Rodinia supercontinent, a part of which resurfaced during mantle upwelling responsible for creating the Cretaceous Ontong Java Plateau.

Keywords: xenoliths; pyroxenite; recycled crust; Ontong Java Plateau; mantle plumes

1. Introduction

Earth's mantle heterogeneity documented by the geochemistry of oceanic basalts such as ocean island basalts (OIB) and mid-ocean ridge basalts (MORB) has been commonly attributed to recycling of crustal materials (e.g. Hofmann, 1997; Stracke et al., 2003) thought to be present as eclogitic/pyroxenitic bodies within the convecting peridotite-dominated mantle (e.g. Allégre and Turcotte, 1986). During the last decade, the role of eclogitic/pyroxenitic sources in the formation of mantle-derived magmas has received an increasing amount of attention in a number of detailed investigations

* Corresponding author. Arthur Holmes Isotope Geology Laboratory, Department of Earth Sciences, Durham University, South Road, Durham, DH1 3LE, UK. Tel.: +44 191 33 42304.
E-mail address: akira.ishikawa@durham.ac.uk (A. Ishikawa).

0012-821X/$ - see front matter © 2007 Elsevier B.V. All rights reserved.
doi:10.1016/j.epsl.2007.04.034

(Hirschmann and Stolper, 1996; Hauri, 1996; Sobolev et al., 2005; Stracke and Sims, 1999). Their relatively low melting temperature, large garnet stability field, and enriched compositions have been considered attractive to explain variations in the physical and chemical characteristics of mantle-derived magmas as part of composite source models (eclogite/pyroxenite incorporated in peridotite). However, their nature, origin, recycling timescales and even their existence remain controversial because the identification of magma sources is not straightforward. For instance, Hauri (1996) presented correlations between major element and isotopic compositions in Hawaiian lavas as robust evidence for the presence of eclogite/pyroxenite in their source mantle. Subsequently, Stracke and Sims (1999) argued against this hypothesis, and attributed the observed isotope and trace element variations to compositionally distinct peridotite components. This contradiction of source identification is largely because the distinct chemical signatures of partial melts derived from different source materials are effectively diluted through magma mixing.

Alternatively, direct mantle samples such as mafic layers in orogenic peridotite massifs (Pearson and Nowell, 2004; Blichert-Toft et al., 1999a) or eclogite xenoliths in kimberlites (Jacob et al., 2005) have been investigated to reveal the isotopic characteristics of eclogitic/pyroxenitic mantle because they are thought to provide an analogue for the aging of old oceanic lithosphere. Moreover, such studies are able to document the spatial extent of isotopic variability and how this correlates with lithological variations. The isotopic compositions of these eclogite xenoliths and pyroxenite layers show extremely large variations relative to those observed in oceanic basalts, reflecting their derivation from ancient subcontinental lithosphere. This suggests that their involvement in basalt source regions in the convective mantle is largely questionable and underlines the importance of natural samples of pyroxenite/eclogite derived from known oceanic locations to better assess the origin of oceanic basalts and heterogeneities in the mantle.

Here we present radiogenic isotope compositions (Sr–Nd–Hf–Pb) of a suite of garnet pyroxenite xenoliths from Malaita, Solomon Islands, as a convincing example of recycled material from within Pacific convective mantle. This argument is founded on three main lines of evidence summarized as follows. First, Malaita represents the southwestern margin of the Ontong Java Plateau (Fig. 1A), which is the largest oceanic plateau, rapidly created on the western Pacific Plate at ca. 120 Ma (e.g. Tejada et al., 2002). The xenoliths were brought up to the surface by a 34-Ma alnöite magma (a silica undersaturated ultramafic magma with an affinity with kimberlite) intruded within the plateau basement,

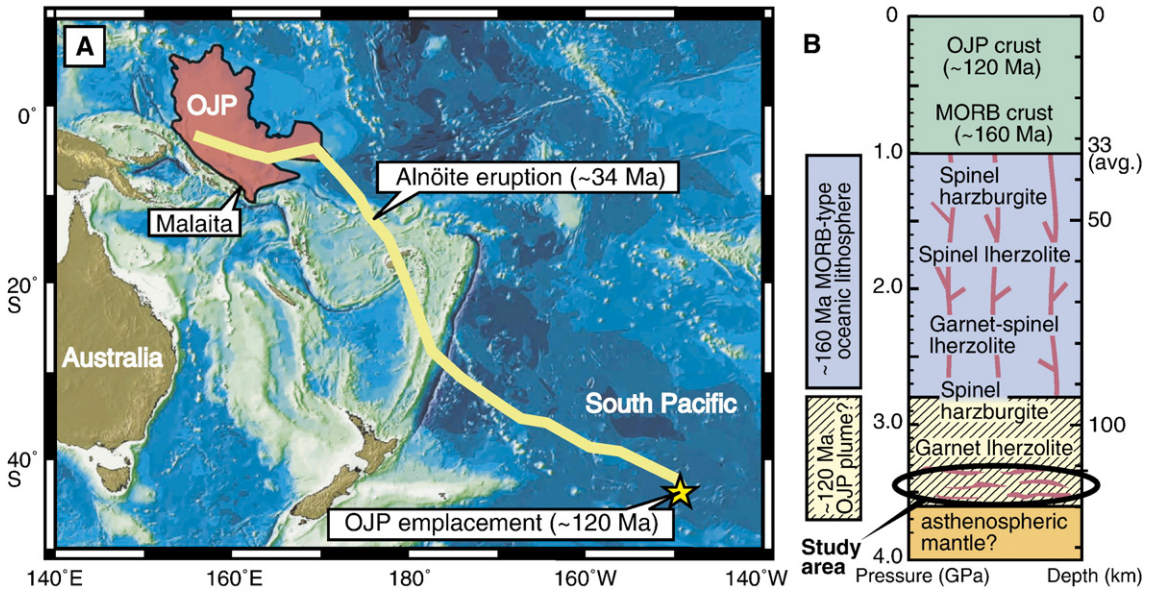

Fig. 1. (A) Location map of Ontong Java Plateau (OJP) and its hypothetical hot spot trail after (Kroenke et al., 2004). The bathymetric map was reproduced from the GEBCO Digital Atlas published by the British Oceanographic Data Centre. Note that the overlying Australian Plate (against Pacific Plate) drifted northeastward from high southern latitudes to present location, indicating that the xenolith entrainment (34 Ma alnöite eruption) occurred in an intraplate setting of the Pacific Basin. (B) Inferred stratigraphic succession beneath the Ontong Java Plateau based on a thermobarometric study of Malaitan xenoliths (Ishikawa et al., 2004). Open ellipse encompasses inferred depths of derivation for garnet clinopyroxenite xenoliths studied here.

Table 1
Trace element concentration data (ppm) for garnet clinopyroxenite xenoliths and the host alnöite from the Malaita, Solomon Islands

Rock	Alnöite[a]		Quartz-garnet clinopyroxenite (QGC)					Bimineralic garnet clinopyroxenite (BGC)			
Sample	SAA1-5 ($n=5$)		SAE116					SAE107			
Phase			Cpx	Grt	Qz	W.R.	$D^{Cpx/Grt}$	Cpx	Grt	W.R.	$D^{Cpx/Grt}$
Mode	W.R. avg.	2σ	0.75	0.21	0.04			0.64	0.36		
Dissolution analyses (ICP MS, TIMS)[b]											
Li	n.a.		9.02	0.715	4.08	7.08	12.6	2.24	0.266	1.53	8.41
Rb	12.9	(19)	0.0084	0.0014	0.0116	0.0071	6.0	0.011	0.0006	0.0073	19
Sr	713	(52)	266	1.54	0.290	200	173	71.0	0.437	45.6	163
Y	27.7	(9)	3.36	26.1	0.0101	8.01	0.129	5.28	36.7	16.6	0.144
Zr	184	(12)	10.2	12.8	n.a.	10.3	0.801	11.7	41.6	22.5	0.281
Nb	109	(66)	0.413	0.113	n.a.	0.333	3.67	0.138	0.076	0.116	1.81
Cs	0.243	(73)	n.d.	n.d.	n.d.			n.d.	n.d.		
Ba	651	(71)	0.692	0.117	0.0853	0.547	5.92	0.570	0.495	0.543	1.15
La	72.5	(21)	2.88	0.050	0.0103	2.17	57.3	0.809	0.014	0.523	56.9
Ce	144	(3)	10.9	0.665	0.0140	8.30	16.4	3.04	0.195	2.01	15.6
Pr	16.3	(8)	1.90	0.233	0.0027	1.48	8.15	0.552	0.078	0.382	7.05
Nd	67.3	(16)	8.25	2.03	0.0109	6.61	4.07	4.06	0.935	2.94	4.35
Sm	12.8	(4)	1.17	0.930	0.0014	1.08	1.26	1.35	0.981	1.22	1.38
Eu	4.00	(16)	0.306	0.376	0.0005	0.308	0.813	0.395	0.528	0.443	0.749
Gd	10.9	(4)	0.941	1.67	0.0015	1.06	0.565	1.26	2.37	1.66	0.530
Tb	1.39	(3)	0.138	0.425	0.0002	0.193	0.325	0.182	0.606	0.334	0.300
Dy	6.37	(13)	0.739	3.61	0.0014	1.31	0.205	1.01	5.36	2.58	0.188
Ho	1.02	(3)	0.117	0.909	0.0003	0.279	0.128	0.174	1.31	0.583	0.132
Er	2.01	(6)	0.285	2.74	0.0008	0.789	0.104	0.391	4.06	1.71	0.096
Tm	0.237	(5)	0.034	0.478	0.0001	0.126	0.070	0.051	0.710	0.288	0.072
Yb	1.30	(4)	0.174	3.27	0.0008	0.817	0.053	0.284	5.05	2.00	0.056
Lu	0.152	(5)	0.021	0.518	0.0001	0.125	0.041	0.034	0.816	0.315	0.042
Hf	3.68	(27)	0.380	0.254	n.a.	0.338	1.49	0.586	1.02	0.744	0.572
Ta	5.4	(29)	0.045	0.0049	n.a.	0.035	9.2	0.015	0.0047	0.011	3.1
Pb	5.57	(9)	0.136	0.010	0.0046	0.104	13	0.033	0.0041	0.022	8.0
Th	10.1	(4)	0.0051	0.0012	0.0001	0.0041	4.1	0.0161	0.0026	0.0112	6.2
U	2.41	(52)	0.0032	0.0028	n.d.	0.0030	1.1	0.0040	0.0042	0.0040	1.0
In situ analyses (SIMS)[c]											
Li			9.5 (1)	0.61 (2)				2.8 (1)	0.27 (4)		
Sr			263 (4)	1.29 (7)				87.1 (10)	0.91 (7)		
Y			3.2 (1)	24.1 (3)				6.3 (2)	41.0 (3)		
Zr			9.3 (3)	11.8 (3)				13.3 (4)	40.7 (3)		
Nb			0.38 (4)	0.10 (1)				0.42 (4)	0.26 (3)		
Ba			0.69 (17)	0.02 (2)				0.19 (6)	0.05 (6)		
La			2.8 (1)	0.054 (11)				0.91 (6)	0.016 (10)		
Ce			10.6 (3)	0.49 (7)				3.4 (2)	0.15 (2)		
Pr			1.9 (1)	0.18 (2)				0.68 (8)	0.063 (6)		
Nd			8.6 (5)	1.6 (3)				4.1 (3)	0.86 (4)		
Sm			1.2 (2)	0.75 (15)				1.4 (2)	0.90 (20)		
Eu			0.31 (5)	0.31 (3)				0.49 (7)	0.48 (7)		
Gd			0.94 (72)	1.5 (4)				1.8 (4)	2.1 (2)		
Dy			0.65 (10)	2.9 (3)				1.3 (2)	5.2 (5)		
Er			0.26 (7)	2.5 (3)				0.46 (11)	4.4 (3)		
Yb			0.16 (6)	2.9 (2)				0.38 (4)	5.4 (3)		
Lu			0.019 (8)	0.40 (6)				0.050 (10)	0.88 (11)		
Hf			0.37 (35)	0.27 (21)				0.74 (62)	2.3 (7)		

Cpx, clinopyroxene; Grt, garnet; Qz, quartz; W.R., whole-rock values calculated from modal estimates and mineral data (excepting elemental concentrations in Qz apart from Li); $D^{Cpx/Grt}$, clinopyroxene/garnet partition coefficients; n.a., not analyzed; n.d., not detected.

[a] Averaged values of five whole-rock measurements are reported. Numbers in brackets are 2σ of five analyses (refer to least significant digits).

[b] Analytical reproducibilities of Rb, Sr, Sm, Nd, U, Th and Pb concentrations with ID-TIMS were typically <0.5% (2σ), whereas elemental concentrations determined with solution ICPMS were generally <5% (1σ) for standard rocks (JB-2 or JB-3). Very low Rb, U, Th and Pb abundances in measured clinopyroxene and garnet may increase estimated errors up to 5% for ID-TIMS and 50% for solution ICPMS.

[c] Numbers in brackets are 2σ of multiple SIMS analyses (refer to least significant digits), which are thought to represent typical errors of analyses. Mass interferences on Sm, Gd and Hf were corrected by assuming constant values of monoxide/metal ratios.

Bimineralic garnet clinopyroxenite (BGC)											
SAE113				SAE120				SAE152			
Cpx	Grt	W.R.	$D^{Cpx/Grt}$	Cpx	Grt	W.R.	$D^{Cpx/Grt}$	Cpx	Grt	W.R.	$D^{Cpx/Grt}$
0.55	0.45			0.54	0.46			0.83	0.17		
3.76	0.388	2.24	9.69	1.44	0.202	0.871	7.12	4.85	0.465	4.11	10.4
0.0051	0.0004	0.0030	12	0.0062	0.0010	0.0038	6.5	0.0076	0.0009	0.0065	8.3
76.9	0.435	42.5	177	83.2	0.420	45.1	198	70.4	0.446	58.5	158
6.04	41.2	21.9	0.146	5.23	37.3	20.0	0.140	3.73	30.8	8.32	0.121
16.0	37.1	25.5	0.430	12.9	42.2	26.4	0.306	11.7	23.1	13.7	0.508
0.252	0.048	0.160	5.19	0.122	0.078	0.102	1.55	0.124	0.050	0.111	2.50
n.d.	n.d.			n.d.	n.d.			n.d.	n.d.		
0.396	0.115	0.270	3.44	0.394	0.048	0.235	8.18	0.208	0.531	0.263	0.391
0.844	0.014	0.470	58.2	1.03	0.016	0.562	65.4	0.693	0.020	0.579	35.2
3.31	0.180	1.90	18.4	3.83	0.182	2.15	21.0	2.56	0.183	2.15	14.0
0.702	0.083	0.423	8.43	0.700	0.074	0.412	9.45	0.482	0.076	0.413	6.36
4.29	0.905	2.77	4.74	4.54	0.931	2.88	4.88	2.98	0.775	2.60	3.84
1.38	0.940	1.18	1.47	1.46	0.985	1.24	1.49	1.12	0.794	1.06	1.41
0.428	0.511	0.465	0.838	0.502	0.541	0.520	0.927	0.315	0.417	0.332	0.754
1.34	2.34	1.79	0.573	1.38	2.45	1.87	0.561	0.966	2.08	1.15	0.465
0.213	0.623	0.397	0.341	0.211	0.628	0.403	0.336	0.131	0.519	0.197	0.252
1.22	5.56	3.17	0.219	1.13	5.21	3.00	0.216	0.753	4.39	1.37	0.171
0.216	1.44	0.766	0.150	0.185	1.34	0.715	0.139	0.125	1.09	0.289	0.115
0.523	4.79	2.45	0.109	0.416	4.09	2.11	0.102	0.275	3.23	0.778	0.085
0.073	0.880	0.436	0.083	0.056	0.756	0.378	0.074	0.034	0.542	0.120	0.062
0.390	6.45	3.12	0.061	0.306	5.60	2.74	0.055	0.166	3.63	0.755	0.046
0.058	1.07	0.514	0.054	0.045	0.925	0.450	0.049	0.022	0.548	0.111	0.039
0.706	0.757	0.729	0.932	0.667	1.02	0.828	0.655	0.581	0.509	0.569	1.14
0.028	0.0029	0.017	9.6	0.016	0.0045	0.011	3.5	0.016	0.0028	0.014	5.8
0.036	0.0037	0.021	9.6	0.036	0.0028	0.021	13	0.032	0.0063	0.028	5.1
0.0094	0.0014	0.0058	6.9	0.0162	0.0034	0.0103	4.8	0.0115	0.0028	0.0101	4.1
0.0030	0.0026	0.0028	1.1	0.0038	0.0038	0.0038	1.0	0.0030	0.0031	0.0030	0.96
3.9 (1)	0.36 (2)			1.6 (1)	0.18 (2)			5.2 (2)	0.45 (3)		
80.3 (9)	0.63 (6)			89.9 (12)	0.60 (3)			67.3 (5)	0.61 (4)		
6.7 (3)	43.5 (4)			6.2 (1)	40.2 (6)			4.1 (2)	32.4 (3)		
17.4 (5)	36.9 (6)			13.8 (5)	42.0 (4)			11.5 (4)	23.5 (4)		
0.21 (2)	0.10 (2)			0.22 (2)	0.11 (2)			0.15 (3)	0.07 (1)		
0.13 (7)	0.03 (5)			0.13 (11)	0.03 (4)			0.12 (6)	0.03 (5)		
0.83 (5)	0.015 (9)			1.0 (1)	0.020 (14)			0.72 (8)	0.018 (15)		
3.3 (2)	0.14 (3)			4.0 (3)	0.15 (3)			2.7 (1)	0.14 (1)		
0.64 (5)	0.065 (13)			0.77 (5)	0.066 (25)			0.53 (4)	0.062 (12)		
4.0 (5)	0.74 (19)			4.5 (6)	0.76 (7)			3.0 (5)	0.72 (19)		
1.4 (4)	0.82 (16)			1.5 (3)	0.89 (18)			1.0 (3)	0.73 (12)		
0.45 (9)	0.40 (4)			0.51 (8)	0.44 (5)			0.34 (4)	0.39 (6)		
1.6 (3)	2.1 (3)			1.6 (4)	2.1 (3)			1.1 (4)	1.8 (4)		
1.2 (2)	5.4 (3)			1.4 (1)	5.1 (3)			0.84 (14)	4.4 (3)		
0.48 (15)	4.7 (5)			0.48 (1)	4.3 (3)			0.31 (8)	3.3 (2)		
0.36 (9)	6.1 (3)			0.37 (1)	5.9 (3)			0.20 (4)	3.9 (3)		
0.043 (13)	1.0 (1)			0.046 (12)	0.98 (14)			0.026 (10)	0.63 (5)		
0.79 (42)	0.95 (86)			0.76 (50)	1.3 (5)			0.52 (40)	0.99 (68)		

essentially in an oceanic setting. This geological evidence indicates that the xenoliths can be regarded as fragments of oceanic lithosphere influenced by the plateau emplacement but never affected by any known subducting slab. Second, thermobarometric analyses of extensive suites of xenoliths (Ishikawa et al., 2004) reveal that virtually the entire lithospheric mantle (Moho to ~120 km in depth) is represented in the xenolith population (Fig. 1B). The suite of garnet pyroxenite xenoliths was sampled from the bottom of the lithosphere (110–120 km in depth) that had accreted to the pre-existing oceanic lithosphere which has a 160-Ma age (Ishikawa et al., 2005). This suggests that isolation of the garnet pyroxenites from the convective mantle occurred between 160 and 34 Ma, probably associated with the 120-Ma plateau emplacement. Third, the extent of petrochemical variation of the garnet pyroxenites is illustrated by the presence of quartz-garnet clinopyroxenite, which has not been recognized in other xenolith suites derived from suboceanic mantle. Typical mantle peridotite cannot melt to produce quartz-normative compositions under high-pressure conditions (>3.0 GPa) and thus excludes derivation of the rock as a high-pressure cumulate or melt from normal peridotitic mantle. This is a clear indication that the rock originated from normative quartz-rich basaltic material, most likely ancient crust stored in the Pacific deep mantle. From these lines of evidence, it is expected that radiogenic isotope data of the garnet pyroxenites can give a unique opportunity to unravel not only the nature and timescale of the recycling process within the Pacific convective mantle, but also the unusual generation of the Ontong Java Plateau.

2. Methods

The samples presented here include one quartz-garnet clinopyroxenite (QGC) and four bimineralic garnet clinopyroxenites (BGC), whose petrographic and major element characteristics, investigated by electron probe microanalysis (EPMA), have already been described (Ishikawa et al., 2004). All preparation and analyses were performed at the Pheasant Memorial Laboratory, Okayama University at Misasa (Nakamura et al., 2003). To avoid the influence of secondary processes that alter the whole-rock compositions (infiltration of host magma, groundwater and seawater), we analyzed Sr, Nd, Hf and Pb isotope compositions and trace element concentrations (including their parent/daughter ratios) of pure clinopyroxene and garnet separates (Pb isotopes were only measured in clinopyroxene) carefully handpicked from the crushed xenoliths. Prior to dissolution, these separates were sequentially acid-leached with 6 M HCl (overnight), 0.5 M HNO_3 (~1 h) and 0.5 M HF (~15 min.) to remove contamination and alteration, and then separated into two or three splits.

The first split (<60 mg) was used for determination of Li, Cs, Ba, rare earth elements (REE) (except for Sm and Nd), Y, U, Th and Pb concentrations by inductively coupled plasma mass spectrometry (ICPMS) using isotope dilution (ID-ICPMS, for Li) and external-standard techniques (Moriguti et al., 2004; Makishima and Nakamura, 1997). The remaining aliquot of the same solution was used to determine Sr and Nd isotope ratios and abundances of Sr, Rb, Nd and Sm by thermal ionization mass spectrometry (TIMS) and isotope dilution-TIMS (ID-TIMS), respectively. The second split (<30 mg) was used for high field strength elements analyses (HFSE: Zr, Nb, Hf and Ta) using an ID-ICPMS technique (Makishima et al., 1999). Samples were decomposed with distilled HF in a Teflon bomb at 245 °C for a week. For clinopyroxene samples, an "Al-addition method" was employed to circumvent isotopic disequilibria of Zr and Hf between sample and spike during the decomposition (Tanaka et al., 2003). On the remaining aliquot of the same solution, Hf isotope measurement was performed with a multi-collector ICPMS (MC-ICPMS) following the method described in (Lu et al., 2007). Determinations of U, Th and Pb abundances and Pb isotope ratios of clinopyroxene were carried out on the third split (200–1000 mg) using ID-TIMS techniques (Kuritani et al., 2006; Kuritani and Nakamura, 2003). Concentrations of U, Th and Pb obtained by ID-TIMS are similar to the results of the solution ICPMS technique mentioned above. Additional Sr and Nd isotope analyses were performed on the residual aliquots after U–Th–Pb measurements and are similar to the results obtained on the split described above. These indicate that the analytical results were virtually unaffected by sample splitting and they must be largely homogeneous. This is supported by the results obtained from *in situ* concentration analyses by secondary ion mass spectrometry (SIMS; Li, Sr, Y, Zr, Nb, selected REE and Hf, analytical procedures outlined in Nakamura and Kushiro, 1998), which yield very low standard deviation of multiple spot analyses, and are in good agreement with data for mineral separates (Table 1).

In addition to the garnet clinopyroxenite xenoliths, five alnöite samples collected from a single outcrop on Malaita were analyzed for Sr–Nd–Hf–Pb isotopes and trace element concentrations. All analyses were performed on dissolutions of whole-rock powder without

Table 2
Rb–Sr, Sm–Nd, Lu–Hf and U–Th–Pb isotope data for garnet clinopyroxenite xenoliths and the host alnöite from the Malaita, Solomon Islands

Rock type	Alnöite [a]		Quartz–garnet clinopyroxenite (QGC)			Bimineralic garnet clinopyroxenite (BGC)											
Sample	SAA1-5 (n=5)		SAE116			SAE107			SAE113			SAE120			SAE152		
Phase	W.R. avg.	2σ	Cpx	Grt	W.R.	Cpx	Grt	W.R.	Cpx	Grt	W.R.	Cpx	Grt	W.R.	Cpx	Grt	W.R.
$^{87}Rb/^{86}Sr$	0.053	(8)	0.0001	0.0026	0.0001	0.0005	0.0039	0.0005	0.0002	0.0029	0.0002	0.0002	0.0066	0.0002	0.0003	0.0059	0.0003
$^{87}Sr/^{86}Sr$	0.704596	(96)	0.707420	0.707431	0.707420	0.703746	0.703808	0.703746	0.704004	0.704009	0.704004	0.703496	0.703519	0.703496	0.705308	0.705444	0.705308
	8		*9*	*9*		*10*	*6*		*8*	*8*		*8*	*9*		*8*	*8*	
$^{87}Sr/^{86}Sr_{(34\ Ma)}$	0.704570	(97)	0.707420	0.707429	0.707420	0.703746	0.703806	0.703746	0.704004	0.704007	0.704004	0.703496	0.703516	0.703496	0.705307	0.705442	0.705308
$^{87}Sr/^{86}Sr_{(120\ Ma)}$					0.707420			0.703746			0.704004			0.703495			0.705307
$^{147}Sm/^{144}Nd$	0.1147	(14)	0.0860	0.2774	0.0984	0.2013	0.6346	0.2510	0.1950	0.6277	0.2587	0.1949	0.6394	0.2610	0.2270	0.6195	0.2469
$^{143}Nd/^{144}Nd$	0.512814	(10)	0.512245	0.512286	0.512247	0.512907	0.513013	0.512919	0.512788	0.512888	0.512803	0.512940	0.513044	0.512956	0.512799	0.512904	0.512805
	4		*8*	*8*		*7*	*8*		*7*	*8*		*6*	*8*		*5*	*8*	
$\varepsilon_{Nd\ (present\text{-}day)}$	3.4	(2)	−7.7	−6.9	−7.6	5.2	7.3	5.5	2.9	4.9	3.2	5.9	7.9	6.2	3.1	5.2	3.2
$^{143}Nd/^{144}Nd_{(34\ Ma)}$	0.512788	(10)	0.512226	0.512224	0.512226	0.512862	0.512872	0.512863	0.512745	0.512749	0.512746	0.512897	0.512902	0.512898	0.512749	0.512766	0.512750
$\varepsilon_{Nd\ (34\ Ma)}$	3.7	(2)	−7.2	−7.2	−7.2	5.2	5.4	5.2	2.9	3.0	3.0	5.9	6.0	5.9	3.0	3.4	3.0
$^{143}Nd/^{144}Nd_{(120\ Ma)}$					0.512170			0.512722			0.512600			0.512751			0.512611
$\varepsilon_{Nd\ (120\ Ma)}$					−6.1			4.6			2.3			5.2			2.5
T_{Sm-Nd} (Ma)					33±22			37.4±9.8			35.3±9.8			35.8±9.5			41±11
$^{176}Lu/^{177}Hf$	0.0059	(5)	0.0080	0.2891	0.0524	0.0082	0.1129	0.0601	0.0116	0.2008	0.1000	0.0096	0.1382	0.0801	0.0053	0.1528	0.0277
$^{176}Hf/^{177}Hf$	0.282943	(7)	0.283255	0.283425	0.283282	0.283021	0.283085	0.283053	0.282872	0.282990	0.282927	0.283086	0.283169	0.283131	0.282971	0.283085	0.282988
	4		*8*	*15*		*19*	*17*		*8*	*6*		*14*	*17*		*24*	*24*	
$\varepsilon_{Hf\ (present\text{-}day)}$	6.0	(2)	17.1	23.1	18.0	8.8	11.1	9.9	3.5	7.7	5.5	11.1	14.0	12.7	7.0	11.1	7.6
$^{176}Hf/^{177}Hf_{(34\ Ma)}$	0.282939	(7)	0.283250	0.283241	0.283249	0.283016	0.283014	0.283015	0.282864	0.282863	0.282864	0.283079	0.283081	0.283080	0.282967	0.282988	0.282970
$\varepsilon_{Hf\ (34\ Ma)}$	6.7	(2)	17.7	17.3	17.6	9.4	9.3	9.3	4.0	4.0	4.0	11.6	11.7	11.7	7.7	8.4	7.8
$^{176}Hf/^{177}Hf_{(120\ Ma)}$					0.283165			0.282918			0.282703			0.282952			0.282926
$\varepsilon_{Hf\ (120\ Ma)}$					16.5			7.8			0.2			9.0			8.1
T_{Lu-Hf} (Ma)					32.4±6.2			33±15			33.4±8.6			35±12			41±13
$^{238}U/^{204}Pb$	30	(6)	1.45 (5)	17.2	1.78	7.74	70.87	11.86	5.30	44.84	8.40	6.66	93.13	11.93	5.96	34.61	7.07
$^{235}U/^{204}Pb$	0.22	(4)	0.0105 (3)	0.125	0.0129	0.06	0.51	0.09	0.04	0.33	0.06	0.05	0.68	0.09	0.04	0.25	0.05
$^{232}Th/^{204}Pb$	128	(6)	2.42 (3)	7.75	2.53	32.21	45.11	33.05	17.26	24.02	17.79	29.10	85.89	32.56	23.80	31.35	24.09
$^{206}Pb/^{204}Pb$	18.840	(21)	17.940 (23)	18.023 [b]	17.942	18.486	18.820 [b]	18.508	18.545	18.754 [b]	18.562	18.434	18.891 [a]	18.462	18.608	18.760 [a]	18.614
$^{207}Pb/^{204}Pb$	15.607	(2)	15.589 (2)	15.593 [b]	15.589	15.555	15.571 [b]	15.556	15.581	15.591 [b]	15.582	15.533	15.554 [a]	15.534	15.581	15.588 [a]	15.581
$^{208}Pb/^{204}Pb$	38.722	(5)	37.695 (21)	37.704 [b]	37.695	38.267	38.289 [b]	38.269	38.267	38.279 [b]	38.268	38.209	38.304 [a]	38.215	38.467	38.479 [a]	38.467
$^{206}Pb/^{204}Pb_{(34\ Ma)}$	18.681	(11)	17.932	17.932	17.932	18.445	18.445	18.445	18.517	18.517	18.517	18.399	18.399	18.399	18.577	18.577	18.577
$^{207}Pb/^{204}Pb_{(34\ Ma)}$	15.599	(2)	15.588	15.588	15.588	15.553	15.553	15.553	15.580	15.580	15.580	15.531	15.531	15.531	15.580	15.580	15.580
$^{208}Pb/^{204}Pb_{(34\ Ma)}$	38.505	(14)	37.690	37.690	37.690	38.213	38.213	38.213	38.238	38.238	38.238	38.160	38.160	38.160	38.426	38.426	38.426
$^{206}Pb/^{204}Pb_{(120\ Ma)}$					17.908			18.285			18.404			18.238			18.481
$^{207}Pb/^{204}Pb_{(120\ Ma)}$					15.587			15.545			15.574			15.523			15.575
$^{208}Pb/^{204}Pb_{(120\ Ma)}$					37.680			38.072			38.162			38.021			38.324

Cpx, clinopyroxene; Grt, garnet; W.R., whole-rock values calculated from modal estimates and mineral data (contributions of quartz in SAE116 were negligible). Data for $^{87}Sr/^{86}Sr$, $^{143}Nd/^{144}Nd$ and $^{176}Hf/^{177}Hf$ are relative to 0.710240 for NBS-987 Sr, 0.511850 for La Jolla Nd and 0.282160 for JMC-475 Hf. Normalizing values for isotopic fractionation corrections are $^{86}Sr/^{88}Sr$=0.1194, $^{146}Nd/^{144}Nd$=0.7219 and $^{179}Hf/^{177}Hf$=0.7325. Numbers in italics for isotope data (except Pb) are internal precisions (2σ mean; refer to least significant digits). Typical external uncertainties on measured $^{87}Sr/^{86}Sr$, $^{143}Nd/^{144}Nd$ and $^{176}Hf/^{177}Hf$ are ±0.000020. Estimated uncertainties on $^{147}Sm/^{144}Nd$ and $^{176}Lu/^{177}Hf$ are <0.5% and <10%, respectively. T_{Sm-Nd} and T_{Lu-Hf} are two-point mineral isochron ages (Ma) calculated with λ values of 6.54×10^{-12} and 1.865×10^{-11}, respectively. Errors are propagated from the above external uncertainties. The ε_{Nd} and ε_{Hf} values are calculated assuming that ε_{Nd} and ε_{Hf}=0 corresponds at the present-day to $^{143}Nd/^{144}Nd$=0.512640, $^{176}Hf/^{177}Hf$=0.282772 and bulk-earth $^{147}Sm/^{144}Nd$=0.1967 and $^{176}Lu/^{177}Hf$=0.0332, respectively. Pb isotope data were corrected with normal double spike and two-double spikes methods (Kuritani and Nakamura, 2003), which yield values of NBS-981 Pb as $^{206}Pb/^{204}Pb$=16.9424, $^{207}Pb/^{204}Pb$=15.5003 and $^{208}Pb/^{204}Pb$=36.7226. Numbers in brackets for Pb isotope data of SAE116 clinopyroxene are 2σ of triplicate analyses (refer to least significant digits), representing typical external uncertainties on the clinopyroxene measurements. Total procedural blanks for all analyses are negligible: 6 pg for Rb, 55 pg for Sr, 0.2 pg for Sm, 2 pg for Nd, 14 pg for Hf, 4 pg for U, 5 pg for Th, and 20 pg for Pb (typical values).

[a] Averaged values of five whole-rock measurements are reported. Numbers in brackets are 2σ of five analyses (refer to least significant digits).

[b] Pb isotope data of garnets were calculated assuming isotopic equilibrium with coexisting clinopyroxenes at 34 Ma.

any leaching process. The techniques used are almost identical to those for clinopyroxene, except that Rb, Sr, Sm, Nd, U, Th and Pb concentrations were determined by solution ICPMS using an external standard. All results are presented in Tables 1 and 2 along with estimated analytical uncertainties, isotopic fractionation corrections and standard values.

3. Mineral equilibria

An apparent lack of compositional gradient in either major or trace element concentrations of minerals within individual xenoliths, revealed by the results of multiple spot analyses with EPMA and SIMS, is thought to reflect their high-temperature equilibration (1300–1350 °C) (Ishikawa et al., 2004). This is further demonstrated by the uniform trace element partitioning behaviors between clinopyroxene and garnet (Table 1, Fig. 2). Our data for clinopyroxene/garnet partition coefficients are comparable to those experimentally determined with similar compositions and conditions (Pertermann et al., 2004; Klemme et al., 2002; Johnson, 1998) and measured by using natural samples such as garnet clinopyroxenite xenoliths from Salt Lake Crater, Hawaii (Bizimis et al., 2005). These exhibit similar overall patterns that appear to decrease progressively from La to Lu with positive Sr, Li and negative Zr anomalies. In detail, however, our data are significantly lower in the heavy REE (HREE) and nearly one order of magnitude higher in Rb, Pb and Sr than the experimentally determined values. By contrast, our partitioning data for HREE, Sr and Pb agree well with those of Salt Lake Crater xenoliths, whose absolute values (except for HREE) are systematically higher than the experimental data. The causes of these discrepancies may be the considerable differences in equilibration conditions (experiments, 1350–1450 °C at ~3.0 GPa; Salt Lake Crater xenoliths, 1200–1300 °C at 2.0–3.0 GPa), and partly due to the uncertainties of attaining equilibrium for highly incompatible elements in synthesized garnet. Although a comprehensive discussion on the variations is beyond the scope of this paper, the broad similarity in their trends and features suggests equilibrium behavior in terms of elemental concentrations.

The attainment of mineral equilibria is also strikingly demonstrated by two-point Sm–Nd and Lu–Hf intermineral isochron ages (Fig. 3). Five Sm–Nd and Lu–Hf garnet–clinopyroxene isochrons give a mean of 35±6 and 35±7 Ma (2σ), respectively, displaying good agreement with the 34-Ma age of host alnöite eruption provided by U-Pb dating of megacrystalline zircon (Davis, 1977). Rb–Sr data do not yield meaningful ages due to low Rb concentrations in both minerals, resulting in similar Sr isotope compositions of garnet–clinopyroxene pairs (Table 2). These data suggest that isotopic equilibrium within individual xenoliths was preserved at the time of host alnöite eruption, and thus whole-rock compositions reconstructed from the mineral data and modal estimates are meaningful in terms of representing their compositional characteristics. It should be noted that the 34-Ma age of mineral isochron does not necessarily represent the timing of pyroxenite formation associated with the host rock magmatism. More likely, it represents continual re-equilibration by inter-mineral diffusion as ambient conditions exceed the blocking temperatures of these isotopic systems. Hence, the isochron ages merely provide another estimate of the eruption age.

This interpretation of the extended residence for the pyroxenites in lithospheric mantle is in line with petrologic indications that the pyroxenites experienced conductive cooling, resulting in subsolidus exsolution of garnet and quartz from liquidus clinopyroxene (Ishikawa et al., 2004). This is supported by the whole-rock trace element characteristics of SAE116 (QGC) and SAE152 (BGC) that show common flattening patterns in the middle and heavy REE (MREE-HREE) range, indicating only minor or no contribution of liquidus garnet to their whole-rock compositions (Fig. 2C). By contrast, typical BGC samples exhibit progressive increase from light REE (LREE) to HREE, suggesting relative accumulation of liquidus garnet. However, present mineral compositions would not represent the "primary" compositions established when the rocks were generated because a decrease in temperature causes significant changes in the modal proportions of garnet and clinopyroxene, and probably their intermineral partitioning behavior. Bearing in mind these considerations, the following discussion will refer to the calculated bulk values to address the origin of the pyroxenites using their isotopic variations.

4. Isotopic variability in garnet clinopyroxenites

In contrast to homogeneous features at the scale of individual xenolith specimens, the reconstructed whole-rock data display significant variations as shown in Sr–Nd–Hf–Pb isotope compositions (Figs. 4–6). It is clear that the QGC has distinctive compositions relative to other BGC. While Sr, Nd, Hf and Pb isotopic variations of BGC are within the OIB-MORB array, the QGC is characterized by remarkably lower $^{206}Pb/^{204}Pb$–$^{143}Nd/^{144}Nd$ and higher $^{87}Sr/^{86}Sr$–$^{207}Pb/^{204}Pb$ ratios, showing some resemblance with EM-1 or DUPAL-type

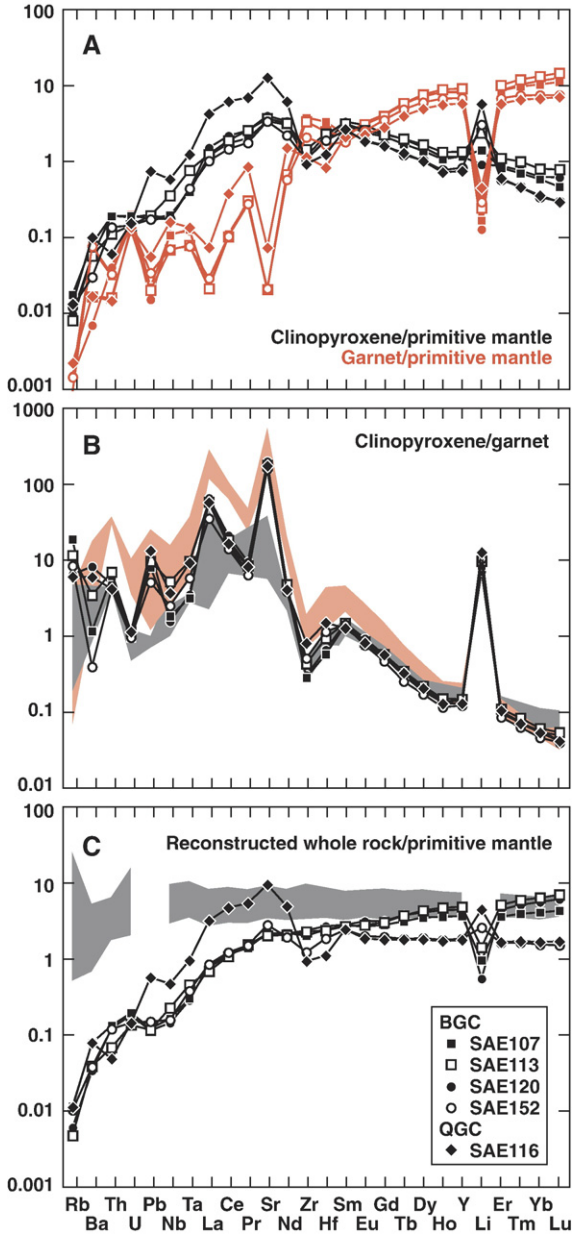

Fig. 2. Primitive mantle-normalized (McDonough and Sun, 1995) trace element patterns for clinopyroxene (black symbols in panel A), garnet (red symbols in A), reconstructed whole-rock (C) and clinopyroxene/garnet partition coefficients (B) of Malaita garnet clinopyroxenites. Grey and red shading in panel B denote clinopyroxene/garnet partition coefficients of experiments (Pertermann et al., 2004; Klemme et al., 2002; Johnson, 1998) and Salt Lake Crater garnet pyroxenites, Hawaii (Bizimis et al., 2005), respectively. Grey shading in panel C is for basalt samples from the Ontong Java Plateau (Fitton and Godard, 2004).

isotopic signatures (Hofmann, 1997; Stracke et al., 2003; Escrig et al., 2004; Hanan et al., 2004). The most striking feature of the QGC can be seen in the ε_{Hf}–ε_{Nd} plot (Fig. 5), in which it displays significant deviation above and to the left of the terrestrial array defined by Hf–Nd isotopic values from a wide variety of crust–mantle samples (Vervoort et al., 1999). These isotopic differences between BGC and QGC can be ascribed to the differing extent of chemical reaction with ambient peridotite in the context of melting of eclogite/pyroxenite bearing mantle according to our previous interpretations (Ishikawa et al., 2004). The petrochemical features of the QGC suggests that its precursor was a high-pressure liquidus clinopyroxene produced by melting of basaltic material after extraction of siliceous melt, and thus the influence of ambient peridotite is apparently negligible. In contrast, the BGC may also represent basaltic residues, but the rocks apparently underwent extensive chemical mass exchange with ambient peridotite through liquid percolation and diffusion in order to reach chemical equilibrium. This is strongly supported by the fact that complementary

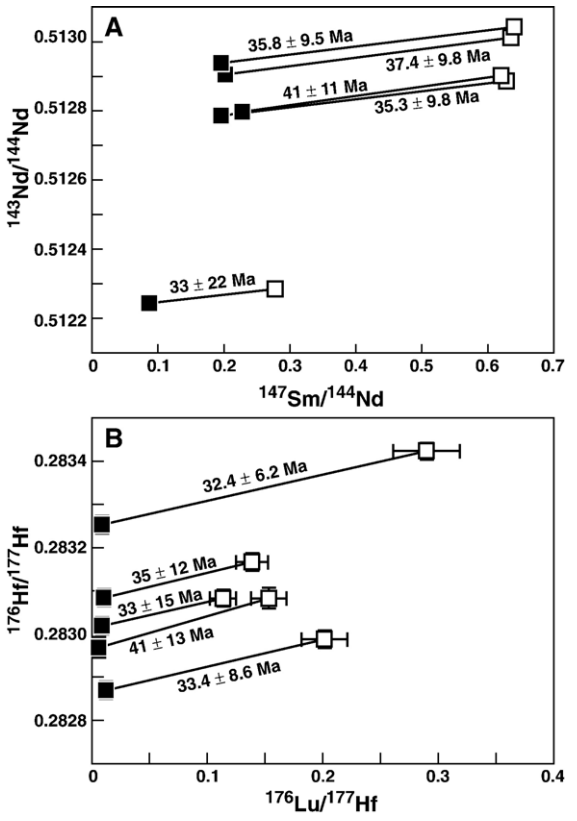

Fig. 3. (A) Sm–Nd and (B) Lu–Hf isotope systematics of Malaita garnet clinopyroxenites. Lines connect the clinopyroxene (solid squares) and garnet (open squares) pair from the same sample. Estimated errors in the ratio determinations are smaller than or equivalent to symbols, except for $^{176}Lu/^{177}Hf$ values of garnet, where error bars are indicated with symbols.

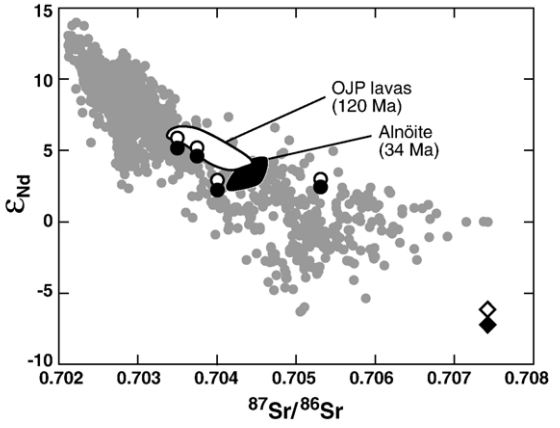

Fig. 4. Sr–Nd isotope compositions of Malaita garnet clinopyroxenite. Calculated whole-rock data of BGC (circles) and QGC (diamonds) are plotted with an age-correction for 34 Ma (open) and 120 Ma (solid). Data sources for oceanic basalts (shaded circles), 120 Ma Ontong Java Plateau (OJP) lavas (open field) and 34 Ma alnöite (solid field) are in (Stracke et al., 2003; Tejada et al., 2004; Ishikawa et al., 2005), respectively.

garnet orthopyroxenite and Fe-enriched garnet lherzolite of assimilative origin intimately coexist together with the garnet clinopyroxenite (Ishikawa et al., 2004). Their constituent phases converge in composition trending towards homogeneity as demonstrated by melting experiments of basalt/peridotite hybrid source (Yaxley and Green, 1998).

It should be noted that the most depleted BGC records very similar Sr–Nd–Hf–Pb isotopic compositions to those of 120-Ma Ontong Java Plateau lavas (Tejada et al., 2004), although its Hf–Nd composition adjusted to 120-Ma plots slightly off the compositional field of the OJP lavas. This similarity suggests that the abovementioned reaction process operated in the framework of the plateau generation. This in turn implies that the Ontong Java Plateau magmatism resulted in melting of eclogite/pyroxenite bearing mantle as proposed by several previous works (Tejada et al., 2002; Ishikawa et al., 2004; Korenaga, 2005). As most previous works on the lavas agree that the major source is peridotite rather than eclogite/pyroxenite Tejada et al., 2004; Fitton and Godard, 2004, the isotopic characteristics of BGC are best explained if the primary enriched signatures of the rocks were largely obscured by the melt-mediated reaction with ambient peridotite of depleted isotopic characteristics. Therefore, it is difficult to assess the primary isotopic composition of individual BGC, as well as ambient peridotite whose isotopic compositions deviate from lava compositions toward more depleted values. A further difficulty in assessing their primary isotopic compositions arises because the initial Hf–Nd data (adjusted to 120 Ma) is variable, probably resulting from an invalid assumption of closed

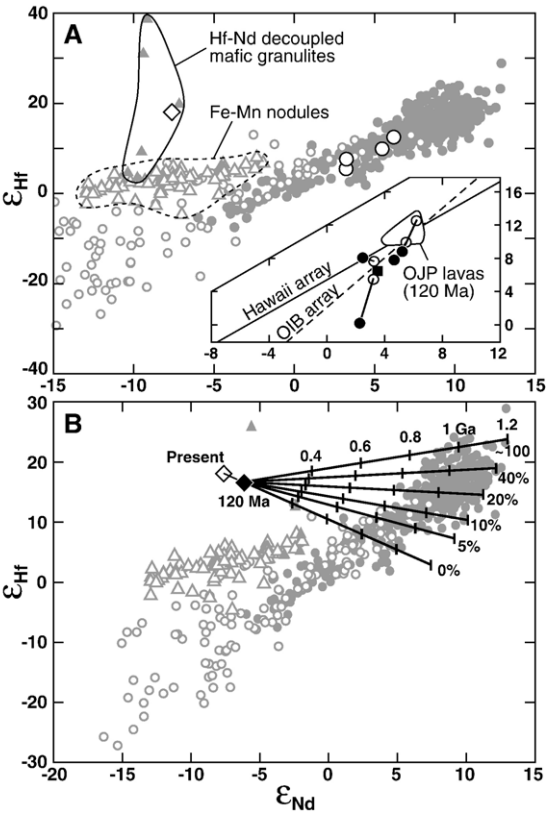

Fig. 5. Hf–Nd isotope compositions of Malaita garnet clinopyroxenites. (A) Present-day calculated whole-rock data of BGC (circles) and QGC (diamonds) are compared to present-day compositions of oceanic basalts (shaded circles), modern and ancient sediments (shaded open circles), ferromanganese nodules (shaded open triangles encompassed by dashed line) and Hf–Nd decoupled mafic granulite xenoliths (shaded triangles encompassed by solid line) (Schmitz et al., 2004; Vervoort et al., 2000). Inset shows the enlargement of evolutionary paths for BGC (present-day, open circles; 120 Ma, solid circles) based on their present-day Lu–Hf and Sm–Nd compositions, compared to 120 Ma Ontong Java Plateau (OJP) lavas (Tejada et al., 2004), 34 Ma alnöite (solid square) and arrays of Hawaii and OIB (Blichert-Toft et al., 1999b). (B) Evolutionary paths (0–1.2 Ga) for QGC are estimated by assuming that Lu/Hf and Sm/Nd ratios were modified by extraction of equilibrated batch melt at 120 Ma. Bold lines represent different trajectories before 120 Ma according to fractions of extracted melt (0–100 %). Background plots are almost identical to those in (A), excepting initial ε_{Nd} and ε_{Hf} for ancient sediments and the mafic granulites. All plots in both figures are relative to $^{143}Nd/^{144}Nd = 0.511850$ for La Jolla Nd and $^{176}Hf/^{177}Hf = 0.282160$ for JMC-475 Hf. ε_{Nd} and ε_{Hf} values are recalculated assuming that ε_{Nd} and $\varepsilon_{Hf} = 0$ today corresponds to $^{143}Nd/^{144}Nd = 0.512640$, $^{176}Hf/^{177}Hf = 0.282772$ and bulk-earth $^{147}Sm/^{144}Nd = 0.1967$, $^{176}Lu/^{177}Hf = 0.0332$. Although complete data sources are too numerous to be cited here, most of them can be found in (Vervoort et al., 1999; Blichert-Toft et al., 1999b; Vervoort et al., 2000).

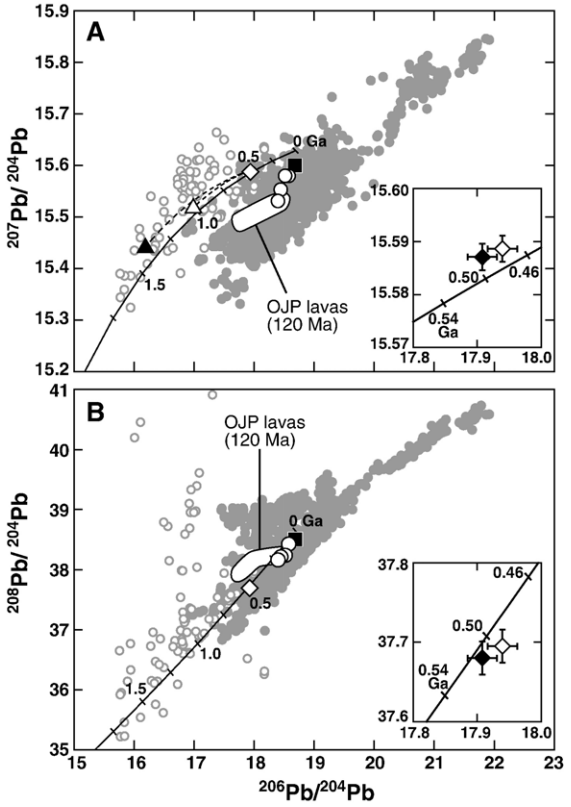

Fig. 6. Pb isotopes of the Malaita garnet clinopyroxenites. Initial compositions of measured clinopyroxenes (BGC, circles; QGC, diamond) at 34 Ma are compared to 120 Ma Ontong Java Plateau (OJP) lavas (Tejada et al., 2004) and 34 Ma alnöite (solid square) in $^{207}Pb/^{204}Pb$–$^{206}Pb/^{204}Pb$ (A) and $^{208}Pb/^{204}Pb$–$^{206}Pb/^{204}Pb$ (B) space. Global compilations of oceanic basalts (shaded circles) (Stracke et al., 2003) and Proterozoic granulites (shaded open circles) (Rudnick and Goldstein, 1990) are shown for reference. Bold curves represent the evolution of Stacey–Kramers Pb (Stacey and Kramers, 1975). Tick marks on the curves (intervals of 0.25 Gy) indicate its Pb isotope compositions in the past. Inset shows the enlargement of the data of QGC, which fits well in ca. 0.5 Ga compositions of the Stacey–Kramers evolution model. Error bars (2σ of triplicate analyses) indicate that the present-day values of measured clinopyroxene (open diamond) and calculated whole-rock values at 120 Ma (solid diamond) are almost identical due to very low present μ and ω values. Note that the large uncertainty of clinopyroxene-melt U, Th and Pb partitioning impedes the assessment of the Pb isotope evolution before 120 Ma, unlike Hf–Nd isotopes. If the 120-Ma melt extraction event resulted in preferential removal of U relative to Pb according to D_U/D_{Pb}=0.25–0.3 (Pertermann and Hirschmann, 2002; Watson et al., 1987), maximum primary μ values of 6–7 make the initial Pb composition approach the 1- to 1.5-Ga point of the Stacey–Kramers curve in the appropriate time interval (open triangle, μ=6 at 1.0 Ga; solid triangle, μ=7 at 1.5 Ga). However, μ=6–7 is too high relative to those of lower crustal mafic granulites with anhydrous mineral assemblages (Rudnick and Goldstein, 1990).

system behavior prior to the xenolith entrainment at 34 Ma (Fig. 5A, inset). Subsequent open system evolution, presumably activated by the presence of stagnated melt, may have significantly altered both isotopic and parent–daughter ratios of the BGC.

5. Origin of quartz-garnet clinopyroxenite

Isotopic characteristics of QGC reflect a long time-integrated evolution with high Rb/Sr–Lu/Hf and low Sm/Nd–U/Pb ratios without recent interaction with ambient peridotite. This is indicated by the preservation of the normative quartz-rich composition of this pyroxenite. When the Hf–Nd data are viewed at 120 Ma, the data somewhat approaches the terrestrial array because of its subchondritic Sm/Nd and superchondritic Lu/Hf ratios (Fig. 5B). This illustrates that present-day parent–daughter ratios predominantly reflect ancient fractionation rather than slight changes resulting from recent melt extraction. Thus, to assess the Hf–Nd isotopic evolution of the QGC, we used simple mass-balance calculations to estimate the possible parent–daughter fractionations during the partial melting process (Table A1). Assuming that the 120-Ma magmatism produced the present whole-rock composition by accumulation of residual clinopyroxene after extraction of equilibrated batch melt, the series of isotopic trajectories before 120 Ma can be approximated with varying fractions of extracted melt, whose trace element concentrations can be assessed by clinopyroxene/melt partitioning data (Johnson, 1998; Pertermann and Hirschmann, 2002). Interestingly, the data devolve

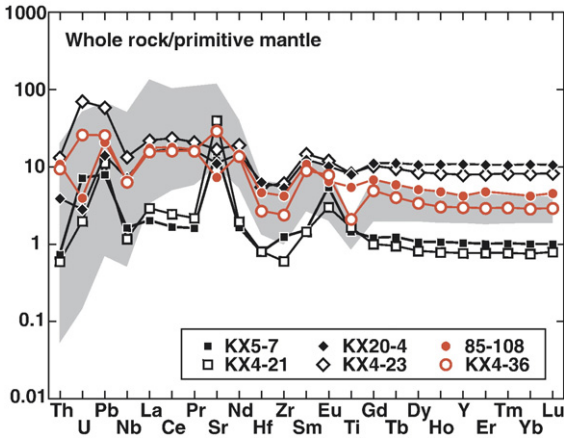

Fig. 7. Primitive mantle-normalized (McDonough and Sun, 1995) trace element patterns for plagioclase-accumulated (square), garnet-accumulated (diamond) and transitional (red circle) types of Hf–Nd decoupled mafic granulite xenoliths (Schmitz et al., 2004; Rudnick and Taylor, 1987). Shaded field is defined by calculated whole-rock data of QGC (lower bound) and coexisting melt compositions estimated by using clinopyroxene/melt partitioning data (Johnson, 1998; Pertermann and Hirschmann, 2002; Watson et al., 1987) (upper bound), which represents the likely compositional range of the QGC protolith.

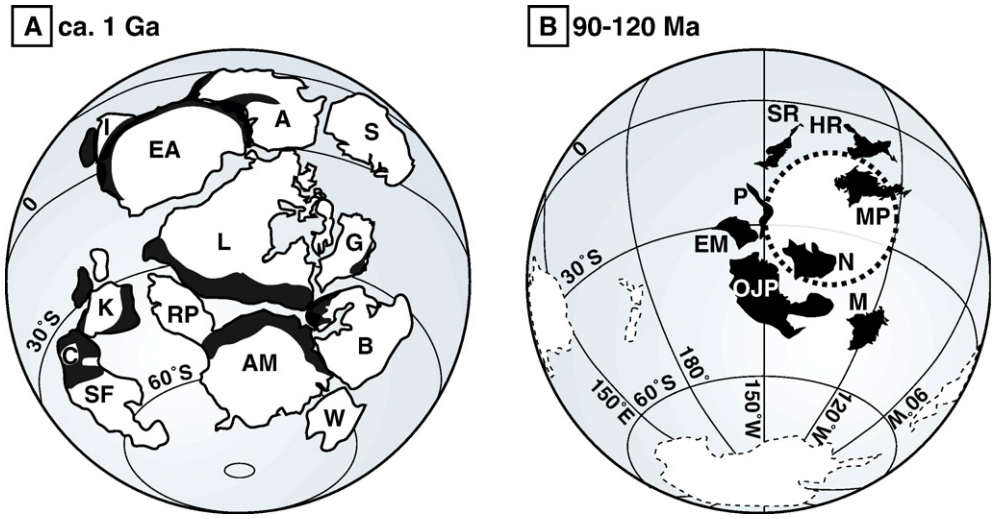

Fig. 8. (A) Paleogeographic reconstruction models of Rodinia at 1010 Ma after (Weil et al., 1998). Grenvillian orogenic belts (1.0–1.1 Ga) highlighted in black after (Hoffman, 1991). A=Australia; B=Baltica; C=Congo; EA=East Antarctica; G=Greenland; I=India; K=Kalahari; RP=Rio de la Plata; S=Siberia; SF=São Francisco; W=West Africa. (B) Paleogeographic reconstruction models of Cretaceous oceanic plateaus during 90–120 Ma after (Lawver et al., 2003). Present locations of continents and Pacific superswell region (Courtillot et al., 2003) are encompassed by thin and thick dashed lines, respectively. EM=East Mariana Basin; HR=Hess Rise; M=Manihiki Plateau; MP=Mid-Pacific Mountains; N=Nauru Basin; OJP=Ontong Java Plateau; P=Pigafetta Basin; SR=Shatsky Rise.

back to the terrestrial array in the upper right quadrant at approximately 1 Ga regardless of extracted melt fraction. This indicates that the QGC acquired anomalous Hf–Nd isotopic compositions as a result of anomalous fractionation of Lu/Hf relative to Sm/Nd at about 1 Ga.

It is well known that due to its chemical robustness, zircon suppresses incorporation of Hf into particulate-water systems, and so the Lu/Hf ratio is fractionated strongly compared to Sm/Nd in the sedimentary system. This results in distinctive compositions between terrigenous (zircon-rich, low-Lu/Hf) and pelagic (zircon-poor, high-Lu/Hf) sediments (e.g. Vervoort et al., 1999). Thus, the Hf–Nd decoupling detected in OIB-MORB magmas is frequently attributed to the recycling of an ancient pelagic sediment component in their sources (Blichert-Toft et al., 1999b; Eisel et al., 2002). Indeed, ferromanganese crusts tend to plot along a trend that deviates obliquely from the terrestrial array, offering a potential explanation for such a slight displacement between Hawaiian and terrestrial arrays (Fig. 5A). However, their extent of Hf–Nd decoupling is too limited to explain the compositions of QGC. On the other hand, similar isotopic evolution and extents of Hf–Nd decoupling among crustal samples have been recently recognized in mafic granulite xenoliths from lower crust beneath southern Africa (Schmitz et al., 2004) and northern Queensland, Australia (Vervoort et al., 2000). It has been suggested that the large decoupling recorded in the whole-rock data of these granulites originates from anomalous parent–daughter fractionations caused by high-grade metamorphism at 1.0–1.1 Ga (Schmitz et al., 2004). Note that the majority of lower crustal granulites studied so far have evolved to present-day isotopic compositions within the terrestrial arrays because most of them are products of juvenile magmatic underplating during Phanerozoic time (Vervoort et al., 2000). This leads to the suggestion that Proterozoic mafic granulites possibly formed by high-grade metamorphism of pre-existing crust, and these granulitic rocks have Hf–Nd isotopic systematics similar to that recorded in QGC.

The similarity of QGC isotope evolution to Proterozoic mafic granulites is further demonstrated by comparisons between elemental concentration data of Hf–Nd decoupled mafic granulites and potential precursor compositions of QGC estimated by the above method (Table A1, Fig. 7). Despite the fact that these mafic granulites could be generated through complex multiple episodes, all of them consistently possess normative quartz-rich basaltic compositions, depletion in HFSE relative to the MREE and enrichment in LREE relative to the HREE (Schmitz et al., 2004; Rudnick and Taylor, 1987). When examined in detail, they can be subdivided into three groups on the basis of their primitive-mantle normalized trace element patterns (Fig. 7). As these lower crustal granulites have been regarded as the deep residues of crustal anatexis

generated during high-grade metamorphism of pre-existing LREE-enriched crustal rocks, such variations are likely to reflect the predominant mineralogy of the residues (Schmitz et al., 2004). The first group (KX5-7, KX4-21) shows a clear signature of plagioclase accumulation represented by positive Sr and Eu anomalies and low-HREE abundances. The second (KX20-4, KX4-23) and third groups (85-108, KX4-36) display very similar trace element patterns but have distinct HREE abundances, possibly reflecting relative differences in the proportion of residual garnet. As can be seen in Fig. 7, trace element characteristics of the third group agree well with the compositional field of QGC protolith, particularly for the sample KX4-36 in terms of absolute abundances of all elements presented. Although detailed trace element modelling to yield the present QGC compositions would be fruitless because of a large degree of flexibility permitted in its protolith composition, this excellent agreement supports the idea that QGC protolith formed through a similar lower crustal differentiation event at around 1 Ga.

Pb isotope compositions of clinopyroxenes add another important piece of information about the nature and differentiation age of QGC because lower crustal granulites have been thought to record a unique Pb isotopic evolution (e.g. Rudnick and Goldstein, 1990). In both $^{207}Pb/^{204}Pb$–$^{206}Pb/^{204}Pb$ and $^{208}Pb/^{204}Pb$–$^{206}Pb/^{204}Pb$ diagrams (Fig. 6), the data of QGC fall in a field defined by Proterozoic granulites with mafic compositions, consistent with the above interpretation. Moreover, the data plot close to the 0.5-Ga point of the Stacey–Kramers Pb evolution curve (Fig. 6, insets), which has been regarded as an evolutionary trace of crustal Pb (Stracke et al., 2003; Stacey and Kramers, 1975). The most straightforward explanation is that the protolith lost U and Th and/or gained crustal Pb at about 0.5 Ga, and subsequent isotopic evolution was hampered by very low μ ($^{238}U/^{204}Pb$) and ω ($^{232}Th/^{204}Pb$) values. This is analogous to the typical Pb isotopic evolution history of Proterozoic mafic granulites, where their Pb isotope compositions may reflect the age of the last tectonothermal or orogenic event that affected the area (e.g. Rudnick and Goldstein, 1990). If this hypothesis is valid, the timing of removal of lower crust into the underlying mantle can be bounded by the minimum isolation age of 0.5 Ga because the subduction of crustal material is an inherent process in active orogenic zones. Even if an alternative transportation mechanism such as lower crustal delamination facilitated by gravitational instability is considered, the situation is unchanged because the process is thought to be restricted to the high-geothermal gradient region that accompanies volcanic activity (Jull and Kelemen, 2001). From these considerations, we envisage that the protolith formation and subsequent subduction/delamination of the QGC occurred during the Neoproterozoic era (0.5–1 Ga).

6. Recycling history of the garnet pyroxenite

The recycling timescale and material documented by the chemical and isotopic compositions of the QGC are consistent with the presence of Neoproterozoic lower crust-like material within the Cretaceous Pacific mantle. This raises the question of how such lower crust material may have been recycled in the context of the geodynamic history of the Pacific region. Based on available geologic records and paleomagnetic data, it has been suggested that a supercontinent Rodinia formed at ca. 1.1 Ga and broke apart at around 0.7–0.8 Ga creating the birth of the Proto-Pacific Ocean (Fig. 8A; e.g. Hoffman, 1991; Weil et al., 1998). Despite considerable uncertainty about the paleogeographic position and configuration of Rodinia (Meert and Torsvik, 2003), most of the 1.0- to 1.1-Ga orogenic belts are proposed to mark the sutures between various elements of the supercontinent. Thus, one possible scenario to account for the recycling of Neoproterozoic lower crust is that Rodinia breakup induced detachment and dispersal of the overthickened suture zone between accreted fragments of the Rodinia supercontinent. This is analogous to recent models suggesting that the breakup of Gondwana played a major role in the pollution of Atlantic-Indian oceanic mantle via lower continental crust delamination (Escrig et al., 2004; Hanan et al., 2004; Kamenetsky, 2001). This scenario is only likely if the present southern Pacific is the site of the Rodinia fragmentation and remains a tentative model requiring further testing.

An alternative scenario to consider is that the pyroxenites investigated in this study were derived from oceanic crustal protoliths comprised of basaltic igneous crust and overlying sediment. If the present southern Pacific was the likely site of Rodinia amalgamation, such materials would be the volumetrically dominant crustal input via pre-collisional subduction of intervening Proterozoic ocean basins. A major drawback of this scenario is that the inferred granulite-grade differentiation is apparently incompatible with the cool geotherms typical of subduction zones (e.g. Peacock, 1993; Schmidt and Poli, 1998). Numerous studies of subduction-related arc magmas suggest that dehydration is responsible for elemental fractionation during cool subduction of the oceanic slab. This selectively retains HFSE due to their lower mobility in slab-derived fluids

and/or strong affinity for a residual Ti-rich phase (e.g. Pearce and Peate, 1995). Thus, a low-HFSE signature in the QGC precludes its derivation from a dehydrated slab. However, it has been suggested that higher geothermal gradients in Precambrian times were not conducive to generating the stability field for blueschists even in a subduction zone setting (Grambling, 1981; Maruyama and Liou, 1998). If the hypothesis of secular cooling is valid, Proterozoic subducting slabs along warm geothermal gradients might have frequently undergone elemental redistribution by partial anatexis, although ubiquitous slab-melting is thought to be restricted in the Archean (Drummond and Defant, 1990). Thus, lower continental crust-like signatures of the pyroxenite do not allow us to strictly rule out their derivation as ancient subducted oceanic crust.

7. Implications for the Ontong Java Plateau magmatism

Despite the uncertainty in recycling history of the pyroxenites, our data provide the first direct evidence for the existence of ancient crustal material beneath the Ontong Java Plateau. An important question is the role of such ancient material in the generation of the Ontong Java Plateau. Traditionally, Cretaceous oceanic plateaus (Fig. 8B) that are widespread in the present-day western Pacific have been attributed to large-scale mantle plume activity during this period (Larson, 1991a,b). However, the origin of the largest, the Ontong Java Plateau, is still the subject of a major debate in terms of whether melting associated with the high-temperature mantle plume is responsible for the episodic and voluminous magmatism (Ishikawa et al., 2004; Tejada et al., 2004; Korenaga, 2005; Fitton and Godard, 2004). In this regard, two "end-member scenarios" have been invoked: high-temperature melting of peridotite mantle plume (>1500 °C potential mantle temperature) (Fitton and Godard, 2004) or entrainment of eclogite-bearing mantle by passive upwelling (~1300 °C potential mantle temperature) (Korenaga, 2005). The presence of recycled eclogite/pyroxenite in the magma source demonstrated by our results is apparently compatible with the second scenario. However, as previously indicated, the difference in trace element signatures between the pyroxenites and the plateau lavas (characterized by low absolute abundances and nearly flat primitive-mantle normalized pattern) appears to support a composite source for the magmas rather than a pure eclogite/pyroxenite source (Fig. 2C). Given the voluminous emplacement of magma in off-axis mature seafloor (Ishikawa et al., 2005), it is likely that hotter than normal mantle played a role in entrainment of recycled eclogite/pyroxenite because off-axis magma generated from low-temperature mantle would consist of a pure eclogite/pyroxenite-derived melt and/or melt derived from composite sources whose volume is dramatically reduced by pyroxene mineralization (Yaxley and Green, 1998). Thus, we envisage that the generation of the Ontong Java Plateau is due to upwelling of a composite mantle plume, although a quantitative estimate of the potential mantle temperature is clearly required to reach a decisive conclusion. For this purpose, geochemical modelling should be revisited, taking into account the contribution of recycled eclogite/pyroxenite combined with reasonable extents of heterogeneity.

Finally, it is interesting to consider whether the plume initiated from the core-mantle boundary as theoretically predicted (Campbell and Griffiths, 1990; Richards, 1989). Experimental investigations suggest that sinking basaltic crusts, except for the coldest slabs, are likely to be gravitationally trapped at the base of the mantle transition zone (e.g. Litasov et al., 2004). It therefore appears that the granulite-like precursor of the QGC is incompatible with its storage in the lower mantle. Moreover, the notion of a primitive mantle-like source previously invoked to explain the geochemical signatures of the Ontong Java Plateau lavas (Tejada et al., 2004; Fitton and Godard, 2004; Parkinson et al., 2002) must be revaluated because the contribution of recycled eclogite/pyroxenite is critical for this argument. Thus, our results lend no support to the hypothesis of plume initiation at the core-mantle boundary. However, the plume hypothesis may explain the temporal coincidence of surges in the creation of oceanic plateaus with the Cretaceous magnetic superchron (Larson and Olson, 1991). Furthermore, mounting evidence from seismic methods clearly indicates the occurrence of a large-scale low-velocity anomaly in the lower mantle under the superswell region of the south-central Pacific (Romanowicz and Gung, 2002), which is spatially related to the birth place of Cretaceous oceanic plateaus (Larson, 1991a) (Fig. 8B). Thus, on-going research for geochemical evidence of lower mantle and core interaction in plume-related materials is still critical to obtaining a complete understanding of the origin of the low-velocity anomaly, and its role in present hotspots and oceanic plateaus.

Acknowledgements

We are grateful to S. Maruyama, T. Komiya and the Solomon Islands Geological Survey for field assistance and all members of the Pheasant Memorial Laboratory for their technical support. D.G. Pearson, B.N. Nath, A.

Utsunomiya, T. Kogiso and J.J. Mahoney are thanked for their constructive comments on an early version of the manuscript. Reviews by two anonymous referees and editorial handling by R.W. Carlson are greatly appreciated. We also thank C.W. Dale for a final check of the English. This study was supported by the Japan Society for the Promotion of Science (JSPS) for Japanese Junior Scientists to A.I., the program "Center of Excellence for the 21st Century in Japan" and grants from the JSPS to A.M.

Appendix A. Supplementary data

Supplementary data associated with this article can be found, in the online version, at doi:10.1016/j.epsl.2007.04.034.

References

Allègre, C.J., Turcotte, D.L., 1986. Implications of a two-component marble-cake mantle. Nature 323, 123–127.

Bizimis, M., Sen, G., Salters, V.J.M., Keshaw, S., 2005. Hf–Nd–Sr isotope systematics of garnet pyroxenites from Salt Lake Crater, Oahu, Hawaii: evidence for a depleted component in Hawaiian volcanism. Geochim. Cosmochim. Acta 69, 2629–2646.

Blichert-Toft, J., Albarède, F., Kornprobst, J., 1999a. Lu–Hf isotope systematics of garnet pyroxenites from Beni Bousera, Morocco: implications for basalt origin. Science 283, 1303–1306.

Blichert-Toft, J., Frey, F.A., Albarède, F., 1999b. Hf isotope evidence for pelagic sediments in the source of Hawaiian basalts. Science 285, 879–882.

Campbell, I.H., Griffiths, R.W., 1990. Implications of mantle plume structure for the evolution of flood basalts. Earth Planet. Sci. Lett. 99, 79–93.

Courtillot, V., Davaille, A., Besse, J., Stock, J., 2003. Three distinct types of hotspots in the Earth's mantle. Earth Planet. Sci. Lett. 205, 295–308.

Davis, G.L., 1977. The ages and uranium contents of zircons from kimberlites and associated rocks. 2nd International Kimberlite Conference Extended Abstracts. unpaged.

Drummond, M.S., Defant, M.J., 1990. A model for trondjemite-tonalite-dacite genesis and crystal growth via slab melting: Archean to modern comparisons. J. Geophys. Res. 95, 21503–21521.

Eisel, J., Sharma, M., Galer, S.J.G., Blichert-Toft, J., Devey, C.W., Hofmann, A.W., 2002. The role of sediment recycling in EM-1 inferred from Os, Pb, Hf, Nd, Sr isotope and trace element systematics of the Pitcairn hotspot. Earth Planet. Sci. Lett. 196, 197–492.

Escrig, S., Capmas, F., Dupré, B., Allègre, C.J., 2004. Osmium isotopic constraints on the nature of the DUPAL anomaly form Indian mid-ocean-ridge basalts. Nature 431, 59–63.

Fitton, J.G., Godard, M., 2004. Origin and evolution of magmas on the Ontong Java Plateau. In: Fitton, J.G., Mahoney, J.J., Wallace, P.J., Saunders, A.D. (Eds.), Origin and Evolution of the Ontong Java Plateau 229. Geological Society of London, London, pp. 151–178.

Grambling, J.A., 1981. Pressures and temperatures in Precambrian metamorphic rocks. Earth Planet. Sci. Lett. 53, 63–68.

Hanan, B.B., Blichert-Toft, J., Pyle, D.G., Christie, D.M., 2004. Contrasting origins of the upper mantle revealed by hafnium and lead isotopes from the Southeast Indian Ridge. Nature 432, 91–94.

Hauri, E.H., 1996. Major-element variability in the Hawaiian mantle plume. Nature 382, 415–419.

Hirschmann, M., Stolper, E.M., 1996. A possible role for garnet pyroxenite in the origin of the "garnet signature" in MORB. Contrib. Mineral. Petrol. 124, 185–208.

Hofmann, A.W., 1997. Mantle geochemistry: the message from oceanic volcanism. Nature 385, 219–229.

Hoffman, P.F., 1991. Did the breakout of Laurentia turn Gondwana inside out? Science 252, 1409–1412.

Ishikawa, A., Maruyama, S., Komiya, T., 2004. Layered lithospheric mantle beneath the Ontong Java Plateau: implications from xenoliths in alnöite, Malaita, Solomon Islands. J. Petrol. 45, 2011–2044.

Ishikawa, A., Nakamura, E., Mahoney, J.J., 2005. Jurassic oceanic lithosphere beneath the southern Ontong Java Plateau: evidence from xenoliths in alnöite, Malaita, Solomon Islands. Geology 33, 393–396.

Jacob, D.E., Bizimis, M., Salters, V.J.M., 2005. Lu–Hf and geochemical systematics of recycled ancient oceanic crust: evidence from Roberts Victor eclogites. Contrib. Mineral. Petrol. 148, 707–720.

Johnson, K.T.M., 1998. Experimental determination of partition coefficients for rare earth and high-field-strength elements between clinopyroxene, garnet and basaltic melt at high pressure. Contrib. Mineral. Petrol. 133, 60–68.

Jull, M., Kelemen, P.B., 2001. On the conditions for lower crustal convective instability. J. Geophys. Res. 106, 6423–6446.

Kamenetsky, V.S., 2001. Remnants of Gondwanan continental lithosphere in oceanic upper mantle: evidence from the South Atlantic Ridge. Geology 29, 243–246.

Klemme, S., Blundy, J.D., Wood, B.J., 2002. Experimental constraints on major and trace element partitioning during partial melting of eclogite. Geochim. Cosmochim. Acta 66.

Korenaga, J., 2005. Why did not the Ontong Java Plateau form subaerially? Earth Planet. Sci. Lett. 234, 385–399.

Kroenke, L.W., Wessel, P., Sterling, A., 2004. Motion of the Ontong Java Plateau in the hotspot frame of reference: 122 Ma–present. In: Fitton, J.G., Mahoney, J.J., Wallace, P.J., Saunders, A.D. (Eds.), Origin and Evolution of the Ontong Java Plateau 229. Geological Society of London, London, pp. 9–20.

Kuritani, T., Nakamura, E., 2003. Highly precise and accurate isotopic analysis of small amounts of Pb using ^{205}Pb–^{204}Pb and ^{207}Pb–^{204}Pb, two double spikes. J. Anal. At. Spectrom. 18, 1464–1470.

Kuritani, T., Usui, T., Yokoyama, T., Nakamura, E., 2006. Accurate isotopic and concentration analyses of small amounts of Pb using isotope dilution coupled with the double spike technique. Geostand. Geoanal. Res. 30, 209–220.

Larson, R.L., 1991a. Latest pulse of Earth: evidence for a mid-Cretaceous superplume. Geology 19, 547–550.

Larson, R.L., 1991b. Geological consequences of superplumes. Geology 19, 547–550.

Larson, R.L., Olson, P., 1991. Mantle plumes control magnetic reversal frequency. Earth Planet. Sci. Lett. 107, 437–447.

L.A. Lawver, I.W.D. Dalziel, L.M. Gahagan, K.M. Martin, D.A. Campbell, The PLATES 2003 Atlas of Plate Reconstructions (750 Ma to Present Day), PLATES Progress Report No. 280-0703 UTIG Technical Report No. 190 (2003) 97 pp.

Litasov, K., Ohtani, E., Suzuki, A., Kawazoe, T., Funakoshi, K., 2004. Absence of density crossover between basalt and peridotite in the cold slabs passing through 660 km discontinuity. Geophys. Res. Lett. 31, L24607. doi:10.1029/2004GL021306.

Lu, Y.-H., Makishima, A., Nakamura, E., 2007. Purification of Hf in silicate materials using extraction chromatographic resin, and its application to precise determination of $^{176}Hf/^{177}Hf$ by MC-ICP-MS with ^{179}Hf spike. J. Anal. At. Spectrom. 22, 69–76.

Makishima, A., Nakamura, E., 1997. Suppression of matrix effects in ICP-MS by high power operation of ICP: application to precise determination of Rb, Sr, Y, Cs, Ba, REE, Pb, Th and U at ng g^{-1} levels in milligram silicate samples. Geostand. Newsl. 21, 307–319.

Makishima, A., Nakamura, E., Nakano, T., 1999. Determination of Zirconium, Niobium, Hafnium and Tantalum at ng g-1 levels in geological materials by direct nebulisation of sample HF solution into FI-ICP-MS. Geostand. Newsl. 23, 7–20.

Maruyama, S., Liou, J.G., 1998. Initiation of ultrahigh-pressure metamorphism and its significance on the Proterozoic–Phanerozoic boundary. Island Arc 7, 6–35.

McDonough, W.F., Sun, S.-S., 1995. The composition of the Earth. Chem. Geol. 120, 223–253.

Meert, J.G., Torsvik, T.H., 2003. The making and unmaking of a supercontinent: Rodinia revisited. Tectonophysics 375, 261–288.

Moriguti, T., Makishima, A., Nakamura, E., 2004. Determination of lithium contents in silicates by isotope dilution ICP-MS and its evaluation by isotope dilution thermal ionisation mass spectrometry. Geostand. Geoanal. Res. 28, 371–382.

Nakamura, E., Kushiro, I., 1998. Trace element diffusion in jadeite and diopside melts at high pressures and its geochemical implication. Geochim. Cosmochim. Acta 62, 3151–3160.

Nakamura, E., Makishima, A., Moriguti, T., Kobayashi, K., Sakaguchi, C., Yokoyama, T., Tanaka, R., Kuritani, T., Takei, H., 2003. Comprehensive geochemical analyses of small amounts of extraterrestrial samples for the analytical competition related to the sample-return mission, MUSES-C, Inst. Space Astronaut. Sci. Rep. SP 16, 49–101.

Parkinson, I.J., Schaefer, B.F., Arculus, R.J., 2002. A lower mantle origin for the world's biggest LIP? A high precision Os isotope isochron from Ontong Java Plateau basalts drilled on ODP Leg 192. Geochim. Cosmochim. Acta 66, A580 (Supplement).

Peacock, S.M., 1993. The importance of blueschist-eclogite dehydration reactions in subducting oceanic crust subduction-zone processes. Geol. Soc. Amer. Bull. 105, 684–694.

Pearce, J.A., Peate, D.W., 1995. Tectonic implications of the composition of volcanic arc magmas. Annu. Rev. Earth Planet. Sci. 23, 251–285.

Pearson, D.G., Nowell, G.M., 2004. Re-Os and Lu–Hf isotope constraints on the origin and age of pyroxenites from the Beni Bousera peridotite massif: implications for mixed peridotite-pyroxenite mantle sources. J. Petrol. 45, 439–455.

Pertermann, M., Hirschmann, M., 2002. Trace-element partitioning between vacancy-rich eclogitic clinopyroxene and silicate melt. Am. Mineral. 87, 1365–1376.

Pertermann, M., Hirschmann, M., Hametner, K., Günther, D., Schmidt, M.W., 2004. Experimental determination of trace element partitioning between garnet and silica-rich liquid during anhydrous partial melting of MORB-like eclogite. Geochem. Geophys. Geosys. 5, Q05A01. doi:10.1029/2003GC000638.

Richards, M.A., 1989. Flood basalts and hot-spot tracks: plume heads and tails. Science 246.

Romanowicz, B., Gung, Y., 2002. Superplumes from the core-mantle boundary to the lithosphere: implications for heat flux. Science 296, 513–516.

Rudnick, R.L., Goldstein, S.L., 1990. The Pb isotopic compositions of lower crustal xenoliths and the evolution of lower crustal Pb. Earth Planet. Sci. Lett. 98, 192–207.

Rudnick, R.L., Taylor, S.R., 1987. The composition and petrogenesis of the lower crust: a xenolith study. J. Geophys. Res. 92, 13981–14005.

Schmidt, M.W., Poli, S., 1998. Experimentally based water budgets for dehydrating slabs and consequences for arc magma generation. Earth Planet. Sci. Lett. 163, 361–379.

Schmitz, M.D., Vervoort, J.D., Bowring, S.A., Patchett, P.J., 2004. Decoupling of the Lu–Hf and Sm–Nd isotope systems during the evolution of granulitic lower crust beneath southern Africa. Geology 405, 405–408.

Sobolev, A.V., Hofmann, A.W., Sobolev, S.V., Nikogosian, I.K., 2005. An olivine-free mantle source of Hawaiian shield basalts. Nature 434, 590–597.

Stacey, J.S., Kramers, J.D., 1975. Approximation of terrestrial lead isotope evolution by a two-stage model. Earth Planet. Sci. Lett. 26, 207–221.

Stracke, A., Sims, K.W.W., 1999. Assessing the presence of garnet–pyroxenite in the mantle sources of basalts through combined hafnium-neodymium-thorium isotope systematics. Geochem. Geophys. Geosys. 1, 000013 (Paper number 1999GC000013).

Stracke, A., Bizimis, M., Salters, V.J.M., 2003. Recycling oceanic crust: quantitative constraints. Geochem. Geophys. Geosys. 4, 8003. doi:10.1029/2001GC000223.

Tanaka, R., Makishima, A., Kitagawa, H., Nakamura, E., 2003. Suppression of Zr, Nb, Hf and Ta coprecipitation in fluoride compounds for determination in Ca-rich materials. J. Anal. At. Spectrom. 18, 1458–1463.

Tejada, M.L.G., Mahoney, J.J., Neal, C.R., Duncan, R.A., Petterson, M.G., 2002. Basement geochemistry and geochronology of central Malaita, Solomon Islands, with implications for the origin and evolution of the Ontong Java Plateau. J. Petrol. 43, 449–484.

Tejada, M.L.G., Mahoney, J.J., Castillo, P.R., Ingle, S., Sheth, H.C., Weis, D., 2004. Pin-Pricking the Elephant: evidence on the origin of the Ontong Java Plateau from Pb–Sr–Hf–Nd isotopic characteristics of ODP Leg 192 basalts. In: Fitton, J.G., Mahoney, J.J., Wallace, P.J., Saunders, A.D. (Eds.), Origin and Evolution of the Ontong Java Plateau 229. Geological Society of London, London, pp. 133–150.

Vervoort, J.D., Patchett, P.J., Blichert-Toft, J., Albarède, F., 1999. Relationships between Lu–Hf and Sm–Nd isotopic systems in the global sedimentary system. Earth Planet. Sci. Lett. 168, 79–99.

Vervoort, J.D., Patchett, P.J., Albarède, F., Blichert-Toft, J., Rudnick, R.L., Downes, H., 2000. Hf–Nd isotopic evolution of the lower crust. Earth Planet. Sci. Lett. 181, 115–129.

Watson, E.B., Ben Othman, D., Luck, J.-M., Hofmann, A.W., 1987. Partitioning of U, Pb, Cs, Yb, Hf, Re and Os between chromian diopsidic pyroxene and haplobasaltic liquid. Chem. Geol. 62, 191–208.

Weil, A.B., Van der Voo, R., Niocaill, C.M., Meert, J.G., 1998. The Proterozoic supercontinent Rodinia: paleomagnetically derived reconstructions for 1100 to 800 Ma. Earth Planet. Sci. Lett. 154, 13–24.

Yaxley, G.M., Green, D.H., 1998. Reactions between eclogite and peridotite: mantle refertilisation by subduction of oceanic crust. Schweiz. Mineral. Petrogr. Mitt. 78, 243–255.